



A Critique on the Role of Object-Oriented Finite Element Analysis (OOF2) in Predicting Thermal and Mechanical Properties in Thermal Sprayed Coatings

Riddhi Joshi¹ · Tanaji Paul¹ · Cheng Zhang¹ · Benjamin Boesl¹ · Arvind Agarwal¹

Submitted: 9 December 2023 / in revised form: 30 May 2024 / Accepted: 31 May 2024
© ASM International 2024

Abstract Microstructural modeling at progressive length scales can enable the prediction of thermal and mechanical properties of thermal sprayed coatings with hierarchical features. Object-oriented finite (OOF2) element modeling conducted using microstructural images, although a powerful technique, has been employed to a limited extent in thermally sprayed materials. Consequently, there is little scientific understanding of the efficiency of the OOF2 technique for estimating bulk properties. For the first time, this study provides a comprehensive analysis of these factors' role in the OOF2 technique's capability to predict thermal and mechanical properties in ceramic and metallic coatings manufactured by plasma spray, high-velocity oxyfuel (HVOF) spray, wire_arc spray, and cold spray. The prediction efficiency generally increases for larger grain sizes as overall microstructural features are captured even at lower magnifications. The same effect is obtained in microstructures having lower and uniformly shaped pores. The data on the porosity suggest that OOF2 predictions are most accurate when conducted on coatings manufactured using sintered feedstock because of the dense powder. In contrast, OOF2 predictions are the least accurate when hollow spherical (HOSP) feedstock having empty cores is used. These multiscale facets of microstructure, porosity, etc., thus, highlight the importance of the selection of the representative volume element for accurate analysis in OOF2, which, depending upon the process, is captured at 300× – 500× for HVOF and wire-arc spray, and

1000× – 15,000× magnifications for plasma and cold spray. This overall assessment charts the relative importance of variables such as grain size, porosity, and feedstock as compared to that of the process and anisotropy in the prediction of properties in thermally sprayed coatings. While these conclusions are based on the limited literature of 37 articles, this study makes a bold attempt towards a guidebook for future thermal spray researchers in conducting more accurate OOF2 analysis.

Keywords microstructure · OOF2 · porosity · property prediction · thermal spray

Introduction

Thermal spraying is a manufacturing technique to deposit metal and ceramic coatings to protect surfaces against thermal, mechanical, and chemical damage. These coatings find extensive applications in aerospace, automotive, and marine components such as turbines, engines, and ballast tanks. Thermal spray is broadly classified into four categories: plasma spray, high-velocity oxyfuel (HVOF) spray, wire_arc spray, and cold spray. In each process, feedstock powder is heated and accelerated onto a substrate, thereby depositing a single building block. A conglomerate of these building blocks, deposited layer by layer, makes up the coating's entirety or 'bulk'. The thermal and mechanical properties of the coatings are prime performance metrics for several applications. However, the experimental measurement of thermal and mechanical properties is challenging due to the difficulty in machining specimens conforming to ASTM size specifications, cost, and time (Ref 1). On the other hand, analytical methods often yield erroneous results due to idealized assumptions, the inability

✉ Arvind Agarwal
agarwala@fiu.edu

¹ Plasma Forming Laboratory, Department of Mechanical and Materials Engineering, Florida International University, 10555 West Flagler Street, Miami, FL 33174, USA

to capture microstructural features, and the lack of feature-specific properties. Computational prediction is an alternative that enables a faster design and optimization of the thermal spraying process. Three-dimensional (3D) finite element modeling (FEM) has been used to predict thermal and mechanical properties. In 3D FEM, the modeled bulk included the property of the overall material instead of individual phases. Those predictions treat thermal sprayed coating as a monolithic material and fail to incorporate hierarchical microstructural features such as splat, oxide, unmelted particles, and porosity. Thus, 3D FEM is more suitable for individual particle analysis and less suitable for the bulk of the coating (Ref 1-3).

Object-oriented finite element analysis (OOF2) is an image-based modeling tool developed by the National Institute of Standards and Technology (NIST) to evaluate heterogeneous materials' overall thermal and mechanical properties. The advantages of OOF2 simulations over conventional techniques are manifold. First, this technique incorporates actual microstructure features into the FEM model (Ref 4). Each microstructural feature's thermal and mechanical properties are assigned to the model from experimentally measured values. Finally, it can conduct the simulations over a large range of length scale of 3 orders of magnitude from a few μm to a few mm, thus providing a comprehensive understanding of multiscale coating properties from local to bulk. Thus, although the analysis begins with 2D images, the relative ease of acquiring microstructures in 3 dimensions and OOFs above capabilities renders it advantageous compared to other FEM techniques. The computed properties are validated with experimental measurements or from values available in the literature. It is noteworthy that experimental validation is required only during the initial protocol development and, once standardized, can drastically reduce experimental iterations.

Due to these advantages, there has been a steady increase in the number of scientific articles published on evaluating thermal sprayed coatings' thermal and mechanical properties, as presented in Fig. 1(a). The complete cluster of these articles was curated from a bibliographic search of Scopus, Google Scholar, and Web of Knowledge databases using keyword criteria of 'Plasma', 'High-velocity oxyfuel', 'Wire arc spray', 'Cold spray', 'OOF', and 'OOF2'. The current literature in this field, from 1999 to the present, comprises 37 articles, in which 74% focuses solely on plasma-sprayed coatings and the rest, 26%, reports on HVOF, wire arc, and cold spray (Fig. 1b). Individually, these articles do not enable a complete understanding of the role of microstructure features and local properties on the ability of OOF2 to yield accurate results. This review is thus a bold first attempt to compare all 37 articles under a single aegis of

microstructure_modeling_property correlations, thus providing a potential roadmap for future researchers and creating a broader landscape of the thermal spray industry.

The OOF2 evaluation of thermally sprayed coatings begins with an image representing the microstructural features of that coating. These microstructural features are unique to the respective coating technique due to the process variables such as temperature and velocity (Fig. 2) (Ref 2, 3). The spraying temperature is high, above the melting point of feedstock in the case of plasma spray, HVOF spray, and wire arc spray, while it is below the melting point of feedstock for cold spray. Similarly, the velocity for cold spray and HVOF spray is high ($>1000 \text{ ms}^{-1}$), while it is low for plasma spray and wire arc spray (Ref 5-13). The variable temperatures and velocities result in unique geometry and sizes of splats, inter-splat boundaries, and volume fraction of porosities in each of the four thermal spray processes, as presented in Fig. 3. In OOF2, these variations translate to significant differences in the calculated bulk thermal and mechanical properties. For example, the thin molten splats in plasma spray result in larger local heterogeneities in stress (Ref 5-9). In contrast, the deformed unmolten splats in cold spray create a more spherical stress distribution (Ref 14-16). OOF2 thus calculates significantly different bulk elastic moduli for the two sprayed coatings. Similarly, the volume of oxides and porosity is relatively low in the case of cold spray, whereas it is relatively higher in wire arc and plasma spray (Ref 5-7, 11-13). These porosities and thermally insulating oxides behave as scattering centers for heat flow; consequently, OOF2 calculates a lower thermal conductivity for the latter processes. Thus, the unique microstructural features of each thermally sprayed coating make a significant impact on the properties calculated by OOF2.

The second input utilized by OOF2 is the local thermal or elastic property of individual features, which is also different in each thermal sprayed process. For example, in plasma, HVOF, and wire arc spray, where the feedstock is melted and resolidified, the local mechanical properties are more akin to cast materials. In contrast, in cold spray, where the feedstock undergoes heavy plastic deformation in the solid state, the local mechanical properties are closer to cold-worked materials. This also holds for thermal properties since melted particles contain a lower concentration of thermal scattering centers such as dislocations. In contrast, cold-sprayed coatings carry a higher density of dislocations (Ref 14-16). OOF2 creates the microstructure-based model that accounts for the phenomenon of heat flux and these defects' scattering in heat flow and consequently calculates lower overall thermal conductivity. Thus, overall, OOF2 models identify individual microstructure features, boundaries between adjacent features, and the corresponding input material properties that are unique to

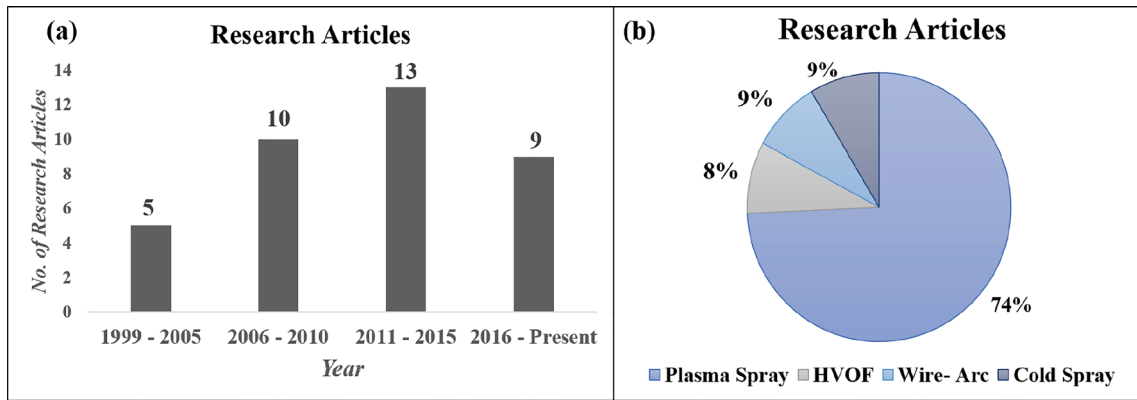


Fig. 1 Current landscape of the scientific literature on properties prediction of thermal sprayed coatings by OOF2. (a) Only 37 articles have been published, growing slowly but steadily from 1999.

(b) Among these, 74% of the articles are focused on plasma-sprayed coatings, while the rest, 26%, are on HVOF, wire-arc-sprayed and cold-sprayed coatings

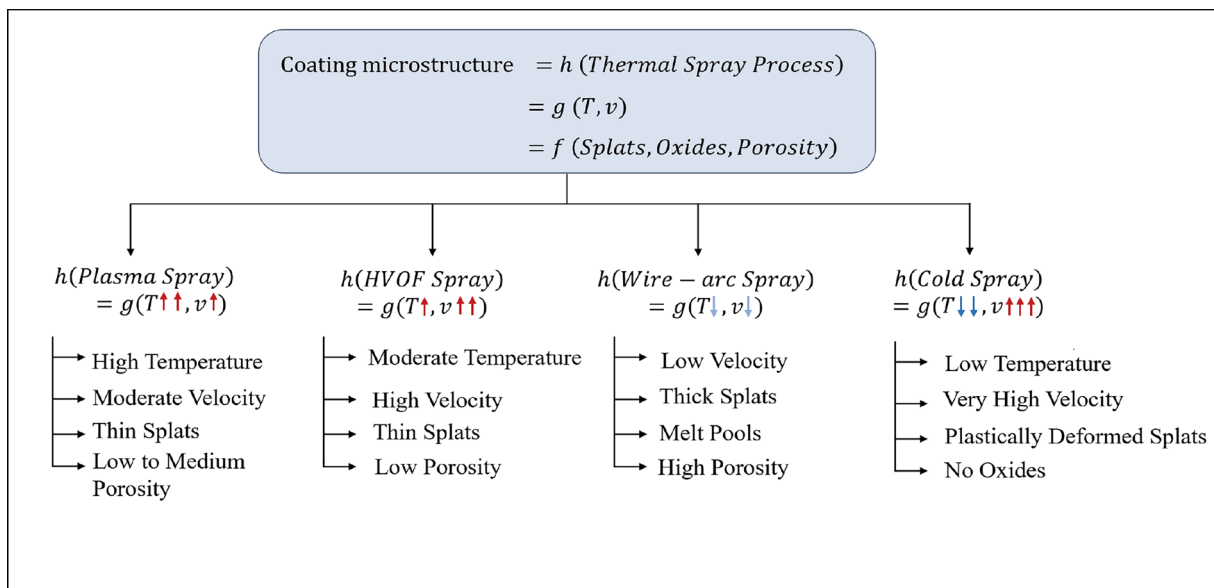


Fig. 2 Variation of process parameters such as temperature (T) and velocity (v) in each thermal spray process. Process temperature is high, above the melting point, for plasma, HVOF, and wire arc spray and below for cold spray. Similarly, process velocity is high for

HVOF and cold spray and low for plasma and wire arc spray. These variations, unique to the spraying process, play a significant role in determining the microstructural features of the coating and, hence, in OOF2 calculations

the feature. The input material property data of these different heterogeneous groups for the OOF2 analysis are user-defined and are obtained from literature sources and/or experimental techniques, as shown in Fig. 4. The sources for values from the previous research literature include published research articles from platforms such as Scopus, Google Scholar, and Science Direct. Additionally, material repositories such as ASM standard property handbooks are also valuable resources for feature-specific property inputs. On the other hand, user-defined inputs from experimental techniques include elastic modulus and thermal diffusivity. Elastic modulus is obtained from instrumented indentation, bending tests, tensile testing, and shear testing, while thermal conductivity is obtained from the laser flash

diffusivity technique. Out of 21 reports on experimental measurement of elastic modulus, a majority of 16 have utilized instrumented indentation techniques. For example, nanoindentation operates on the principles of load-displacement measurements to characterize mechanical properties at nanometer-length scales. Controlled indentation is executed with precise loading and unloading cycles, enabling the acquisition of force-displacement curves. Analysis of these curves yields essential mechanical parameters such as hardness, elastic modulus, and indentation depth. This measured elastic modulus is utilized for OOF2 simulations. With respect to thermal sprayed coatings, nanoindentation provides phase-specific elastic modulus such as that in the interior of splats, inter-

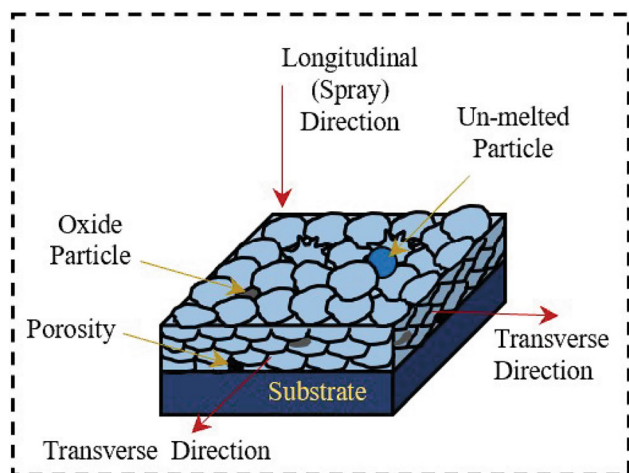


Fig. 3 Schematic of representative microstructure observed in thermally sprayed coatings. The coating, built up as layers on top of the substrate, constitutes unique microstructural features such as splats, inter-splat boundaries, unmolten particles, and porosity. Red arrows mark the spraying direction and transverse directions

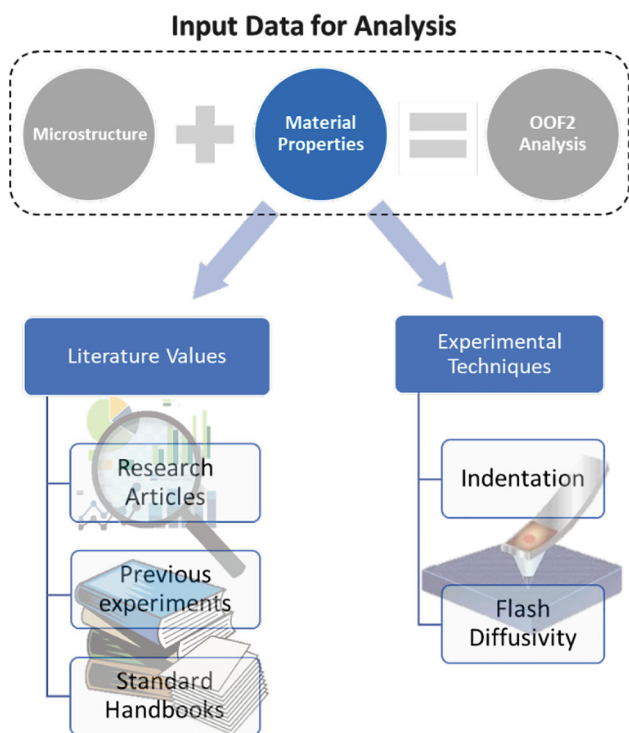


Fig. 4 Classification of material properties database and its sources for user input in OOF2 analysis

splat jetting regions, grain boundaries, and secondary precipitates. Similarly, for experimental measurement of thermal properties, all 11 reports have utilized flash diffusivity analysis to determine thermal diffusivity in materials. It involves subjecting a thin sample to an intense, short-duration heat pulse generated by a xenon flash lamp. The resulting transient temperature rise is measured at

various points along the sample surface using high-speed infrared detectors which are governed by the thermal diffusivity of the material, along with its thermal conductivity and specific heat capacity. Nanoindentation and flash diffusivity analysis represent advanced experimental techniques that provide invaluable insights into the mechanical and thermal properties of materials at the desired length scales for OOF2 simulations.

Finally, OOF2 evaluates overall thermal and mechanical properties *as a function of the length scale*. This means that a mechanical property such as elastic modulus, calculated by OOF2 based on a microstructural image at a 1_millimeter length scale, will be significantly different from that calculated at a 1_micrometer scale. This stems from the influence of microstructural features, such as porosity and cracks, on the material properties of thermal sprayed coatings at various locations and different length scales. However, these differences average out in larger bulk scales (> 10 mm), and OOF2 calculates similar property values to the experimental values. Moreover, the bonding between adjacent layers in the spraying direction differs from that between adjacent splats in the transverse direction. OOF2 creates a model that can incorporate this anisotropy of the material from microstructural images acquired from cross_sections. Thus, OOF2 can solve for the material properties at a wide range of length scales and in different directions of the coating.

The efficiency of OOF2 calculated properties heavily depends on microstructure image quality. These include but are not limited to the unique features of the coatings, such as splats, grain size, oxides, porosity, their individual local properties, and the length scale of evaluation (Ref 17-26). Thus, it is important to identify the critical parameters that influence the microstructure’s quality that influences the prediction efficiency of OOF2. OOF2 validation efficiency refers to ‘the degree to which the result of a calculation conforms to the correct value or a standard’. The experimentally measured value of a property of thermally sprayed coating, such as its elastic modulus or thermal conductivity, is correct or standard. This is due to the fact that prior to conducting an experimental measurement, the instrument is calibrated by testing on standard samples with known properties. Thus, OOF2 validation efficiency is essentially the ratio of the value of a mechanical or thermal property obtained by OOF2 calculations and its corresponding value obtained from experimental techniques, expressed as a percentage.

$$OOF2 \text{ Validation Efficiency} = \frac{\text{Predicted Property value}}{\text{Standard property value}} * 100$$

These properties, such as thermal conductivity, heat flux, stress distribution, and elastic modulus, are critical to the performance of thermally sprayed coatings across a broad

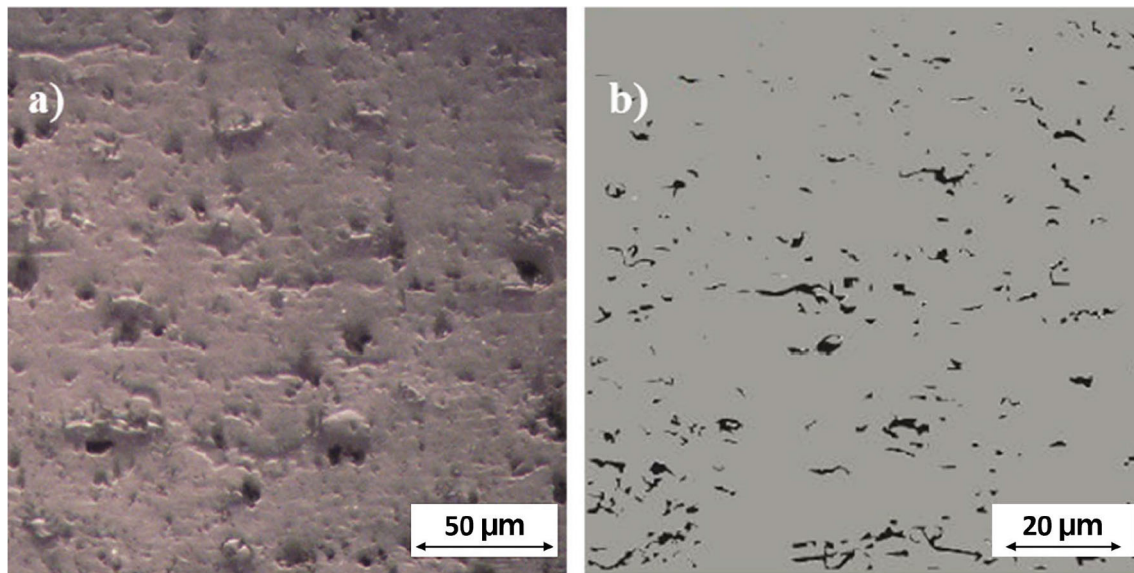


Fig. 5 Comparison of computationally generated microstructure with experimentally acquired one. (a) Experimental microstructure of plasma-sprayed aluminum oxide coating acquired by optical microscopy technique. (b) Computationally generated microstructure obtained by SimDrop 3.0 software using computational fluid dynamics algorithms to generate individual splats stacked together using

spectrum of industries and applications. Thus, it is necessary to establish the correlations between OOF2 calculated properties and their efficiencies with the characteristics above to understand the simulation process scientifically. The present article, an analytical review of OOF2, is thus the first report to bridge this gap in the scientific literature.

Methodology of Finite Element Modeling by OOF2

Acquisition of Microstructure

The most crucial part of conducting a FEM by OOF2 is the acquisition of the microstructure of a thermal sprayed coating at systematically progressing length scales. This can be done by two approaches: experimental and computational. In the first approach, experimental microstructural images are acquired by an optical and/or electron microscope. The images are recorded at multiple magnifications and locations to capture the features of the coating at different length scales. In these multi-length-scale images, OOF2 maintains the original pixel size and quantity in the microstructure, determined by input height and width dimensions at the acquired length scale. Additionally, OOF2 enables the selection and grouping of these pixels corresponding to the diverse phases found in the microstructure. Analysis performed on low-magnification images provides the overview of global material properties, whereas the higher-magnification image analysis provides

stochastic models [6]. Reprinted from *Surface and Coatings Technology*, Vol. 374, Sadhana Bhusal, Cheng Zhang, Jenniffer Bustillos, Pranjali Nautiyal, Benjamin Boesl, Arvind Agarwal, A computational approach for predicting microstructure and mechanical properties of plasma sprayed ceramic coatings from powder to bulk, p. 1-11, Copyright 2019, with permission from Elsevier

the data on single particle/splat microstructural features. The multiscale study also reveals the influence of a single splat on the neighboring elements in the microstructure, thereby correlating the microstructure's local property to the global properties of the coating. Out of 37 articles on OOF2 modeling thermal sprayed coatings, 33 have utilized experimentally acquired microstructures (Ref 26-37).

In contrast to 33 reports on experimentally acquired microstructures, only four reports have utilized computationally generated microstructure images. This involves a bottom-up approach beginning at a small length scale. At this scale, individual splats are simulated by a volume of fluid (VOF) tracking mechanism by varying parameters such as feedstock material and size, spraying temperature and velocity, and substrate pre-heating temperature. These individual splats are arranged over a 2D array to obtain a single coating layer. In the final step, these layers are stacked on top of one another to obtain a microstructure of a bulk coating with the desired thickness, usually in the range of 10-100 µm. This final computationally generated microstructure is akin to that of experimental microscopic techniques. A comparison of computationally generated microstructure with experimentally acquired one is presented in Fig. 5. In this study by Bhusal et al., an optical microscopy technique was employed to obtain the experimental microstructure of plasma-sprayed aluminum oxide coating shown in Fig. 5(a) (Ref 6, 7). The first individual splats were simulated by SimDrop 3.0 software using computational fluid dynamics algorithms in the computational approach. Disk-shaped fingered and fragmented

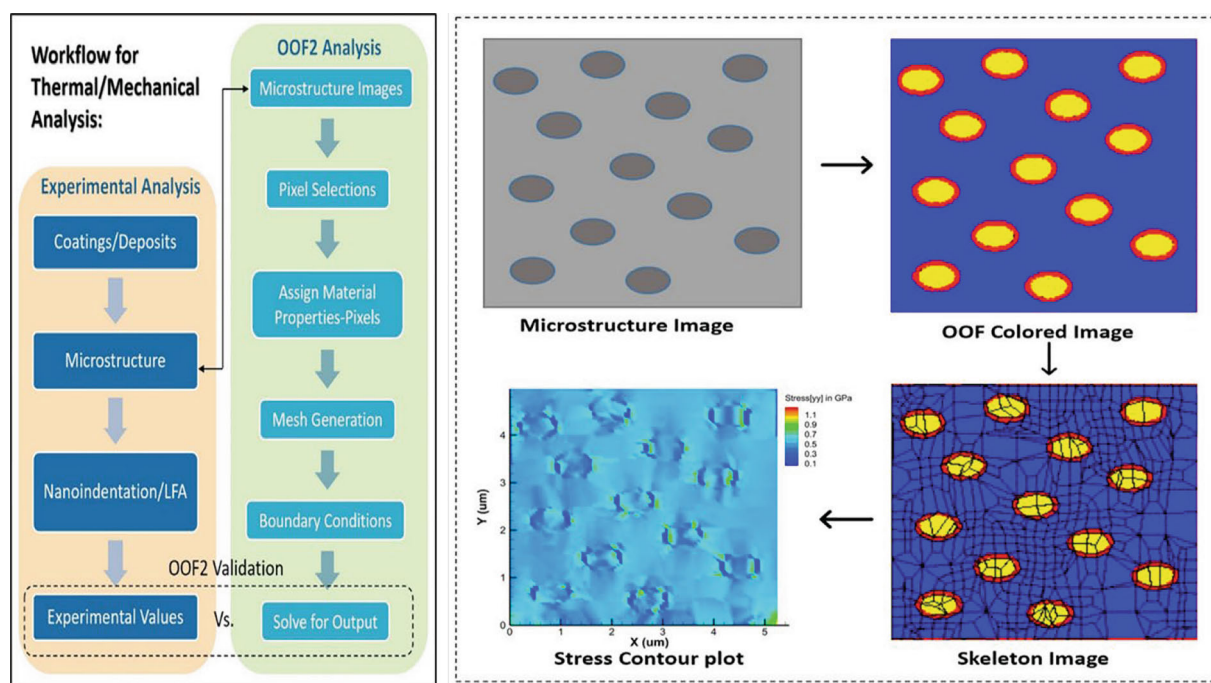


Fig. 6 Analytical workflow and experimental validation process followed by OOF2 for calculating properties of thermally sprayed coatings shown by an (a) flowchart and (b) schematic

splats were simulated using Navier–Stokes equations. These splats were then stacked using a stochastic model to generate a bulk 3D microstructure (Fig. 5b) that shows good agreement with the experimental one (Fig. 5a).

Similarly, Wang et al. generated computed microstructures of plasma-sprayed yttria-stabilized zirconia (YSZ) coatings using small-angle neutron scattering (SANS) information. The microstructure, pores, voids, and cracks were synthetically constructed and perfected using volumetrically averaged information obtained from SANS (Ref 24). Among the other 2 studies, Ghafouri-Azar et al. have used a 3D stochastic model to generate HVOF-sprayed stainless steel and tungsten carbide coatings (Ref 8). Gupta et al. have used Tbxtool software to generate HVOF-sprayed YSZ coatings (Ref 34).

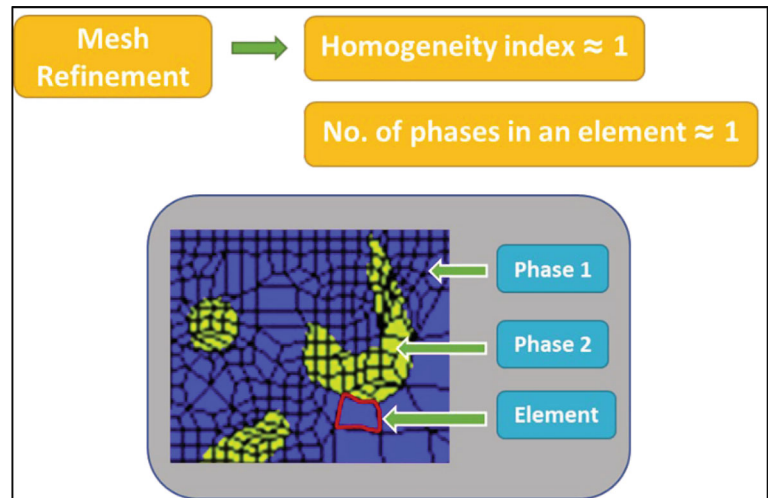
Analytical Workflow

The methodology for OOF2 begins with the microstructure of the thermally sprayed coatings, progresses through the assignment of properties of individual features, and finally, the solution of relevant equations to obtain the bulk properties. A flowchart and schematic example present the workflow in estimating the coating properties and experimental validation in Fig. 6. First, the coating micrographs are converted into binary images through image analysis software such as ImageJ. This software pixelates individual phases of the heterogeneous microstructure into specific binary colors based on user-defined inputs. OOF2 groups

together these pixels for a named selection of the phases or features, followed by a materials property file assigned to the respective phase/feature. The assigned values for the thermal or mechanical property are user-defined inputs from experimental techniques such as nanoindentation, laser flash diffusivity analysis, published literature, and standard material property handbooks. Next, OOF2 generates a framework of the microstructural image to facilitate meshing. It employs adaptive mesh refinement techniques, including annealing, snapping nodes, swapping edges, and refining. Snapping nodes involves aligning the nodes with the pixel boundaries, ensuring a precise representation of the microstructure. After snapping, annealing adjusts the mesh by relocating nodes that do not meet the user-defined acceptance criterion, termed ‘alpha’. Alpha, a measure that determines the pixel group that a particular pixel in the image is classified into, ranges from 0 to 1.0. It sets the threshold for distinguishing objects from the background based on the grayscale intensity of the pixel. For instance, an alpha of 0.8 categorizes pixels with intensity below 80% of the max as background pixels and above as object. Next, the mesh is further refined by subdividing the elements at the boundary of the individual phases. The internal boundaries of the individual element and the neighboring elements are moved to merge as one boundary, thus reducing the total number of phases in the elements, as shown in Fig. 7.

The swapping edges technique involves iteratively examining the edges of an element within the mesh and swapping

Fig. 7 Significance of Mesh Refinement and Homogeneity Index in OOF2 Analysis



them to improve the quality of the mesh. The criteria for swapping edges can include considerations such as minimizing element distortion and or reducing the number of phases within an element to one. This defines the homogeneity of the simulation, which is the deciding factor for the quality of the mesh of elements. While a homogeneity index of 1 is ideal, those in the range of 0.95 to 0.99 yield good results (Ref 4, 6). As mentioned earlier, the homogeneity index measures the number of phases in one element contributing to the microstructure's generated mesh. Thus, the microstructures with complex geometries, a dominance above 95% of one phase in the element, create an accurate mesh to yield results closest to experimental data (Ref 6-9). A homogeneity index of 0.99 is preferred for greater prediction efficiency. However, it is not recommended to create an extremely fine mesh where the element size equals pixel size in the microstructure as it can capture features such as noise that are not part of the coatings. After the mesh is generated, boundary conditions are applied to the microstructure to evaluate the material properties. OOF2 solves user-defined fields and equations for boundary conditions such as displacement, temperature, voltage, heat equation, plane heat flux, force balance, and plane stress (Ref 4). The most common bulk coating properties evaluated are effective thermal conductivity and elastic modulus. The computed values can be validated against experimental results from nanoindentation, uniaxial tensile testing, and laser flash diffusivity analysis to validate predicted OOF2 results.

Data Extraction Strategy for this Analytical Review

This analytical review focuses on the efficiency of OOF2 calculations concerning the different microstructural aspects, such as grain size and porosity. Since this

information is not directly reported, exhaustive data mining was conducted on all 37 published articles to extract the relevant information below (*Data files are attached as supplementary files.*) However, it is important to note that the total number of published articles is not directly associated with the total number of data points in the plots discussed in the results and discussion section. The published articles may contain more than one data point depending on the number of materials and properties being analyzed. For example, an article with two materials analyzed to predict thermal and mechanical properties will have 4 data points for 1 published article.

Grain Size Measurement

The grain size of thermal sprayed coatings was calculated using micrographs by image analysis. As shown in Fig. 8, the grain, length, and width measurements were recorded manually using ImageJ. (*The data files for microstructure images are available on GitHub.*) To enable accurate measurements, the contrast of images was enhanced, and ImageJ was used to segment them into regions demarcating grains and their boundaries/interface regions. The arithmetic mean of length and width was recorded for 5-7 grains for each microstructure. The average of these 5 to 7 measurements is the calculated average grain size of the microstructure $(L + W)/2$. It is noteworthy here that a thermally sprayed splat is usually constituted on multiple grains. Since the calculation of grain size is a two-dimensional image-based analysis, the flattening of the splat is not included in the measurement of the average grain size.

OOF2 Validation Efficiency Calculation

The 'validation efficiency' of OOF2 simulations is presented as the parameter calculated from each of the 37

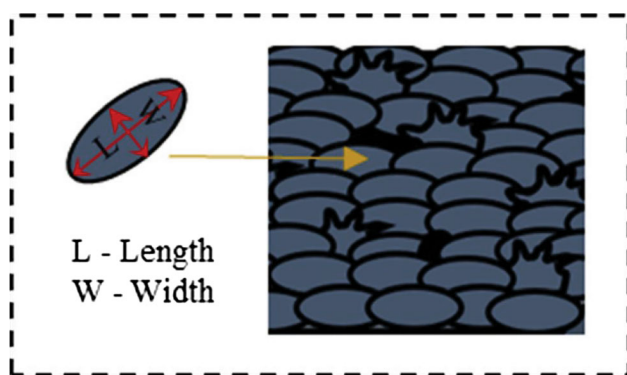


Fig. 8 Method employed in this study for extracting information on the grain size of thermally sprayed coatings from all of the 37 research articles published to date. To obtain a size representative of the entire coating, 5-7 length and width measurements were recorded per microstructure. The average of these is used to plot the X-axis of the following graphs

articles. It is defined as the percentage ratio of the value calculated by OOF2 concerning that measured by the experiment. This value in percentage is plotted on the Y-axis (ordinate). An identical match of the predicted value with an experimentally measured one yields a validation efficiency of 100%. An overestimation or underestimation yields values higher or lower value than 100%, respectively. A more significant deviation from 100%, lower or higher, represents an inefficiency of OOF2 predictions.

Microstructural data such as porosity percent and average grain size were plotted on the horizontal X-axis, while OOF2 validation efficiencies were plotted on the vertical Y-axis. The porosity values were taken as reported in the literature. Validation efficiencies from OOF2 thermal analysis were plotted against the grain size and porosity of ceramics and metallic coatings. Those obtained for the mechanical properties' estimation were plotted only against grain size. This is because the data on porosity content in the microstructure are only reported for 9 studies out of 23 data points available in the literature, thus restricting the analysis. The number of articles mined for constructing these relationships is presented in the flowchart in Fig. 9. Here in the flowchart below, 'n' represents the total number of data points of porosity and grain size plotted against OOF validation for each material as discussed in results and discussion section.

Results and Discussion

This section establishes the correlations between the efficiency of OOF2 property predictions concerning microstructural features, grain size, and porosity. These outcomes are broadly divided into two significant investigations: thermal and mechanical analyses. Since the type of

the material controls the results and their dependence on coating features, each is further subdivided into ceramic and metallic coatings.

OOF Prediction of Thermal Properties in Ceramic Coatings

Thermal conductivity is the most assessed thermal property of plasma-sprayed ceramic coatings by OOF2. Thermal conductivity is inversely affected by interfacial thermal resistance, known as Kapitza, contact, and air resistance (Ref 6). Thermal resistance at the boundary of two splats measures resistance to heat flow through them. This resistance plays a significant role in transferring heat flux through the system. Additionally, contact resistance between the splats results from heat flux scattering at the immediate interface, whereas air resistance is observed due to the absence of material resulting in pores. Interfaces such as splat_splat and splat_coatings, and the remaining data points porosity affect the overall thermal resistance of the material more significantly at the microscale due to the collective effect of the resistance at the given magnification. Thus, to accurately capture the effect of these resistances on the overall conductivity of the coating, it is essential to select a representative microstructure that retains all the features, such as porosity, interfacial regions, and grain sizes at different lengths scales.

It is noted that 97% of the thermal analysis of ceramic deposits studies is on ZrO_2 (zirconia) coatings, and the remaining data points are for alumina coatings (Al_2O_3) (Ref 5, 6, 17-42). The data points on OOF2 predictions of thermal sprayed ceramic coatings from the literature were plotted against the average *grain size* of the microstructure, as shown in Fig. 10. Upon assessment of this figure, it was observed that for larger grain sizes of 8-50 μm , OOF2 validation was better (70-110%) than that for smaller grain sizes of 2-4 μm (underestimation of 39% and overestimation of 160%). This is because the OOF2 analysis is a microstructure-based tool, and its efficiency depends on the ability to distinguish and identify between different heterogeneous phases. The heterogeneous phases of large grain sizes are easy to distinguish. In contrast, the resolution of microstructure with smaller grain sizes is comparatively lower, thus yielding lower OOF2 validation efficiency. However, it could be improved if higher-magnification images with better resolution could be used as input. The microstructures corresponding to the 33 data points mentioned above are obtained through the air plasma spray (APS), suspension plasma spray (SPS), solution precursor plasma spraying (SPPS), and axial suspension plasma spray (ASPS). Microstructures obtained through each variant of the plasma spray process are different. Air plasma spray (APS) results in a traditional splat-

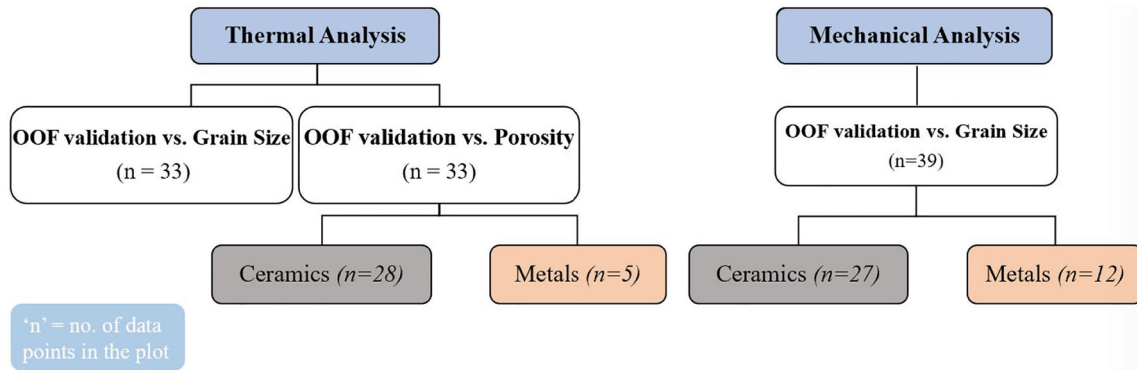


Fig. 9 Flowchart depicting strategy adopted in this analytical review to establish the dependence of microstructural features on the efficiency of calculations conducted by OOF2. Validation efficiencies of thermal analysis were plotted against grain size and porosity, while

those of mechanical analysis were plotted against grain size. Exhaustive data extraction was conducted from all the published research articles mentioned in parentheses

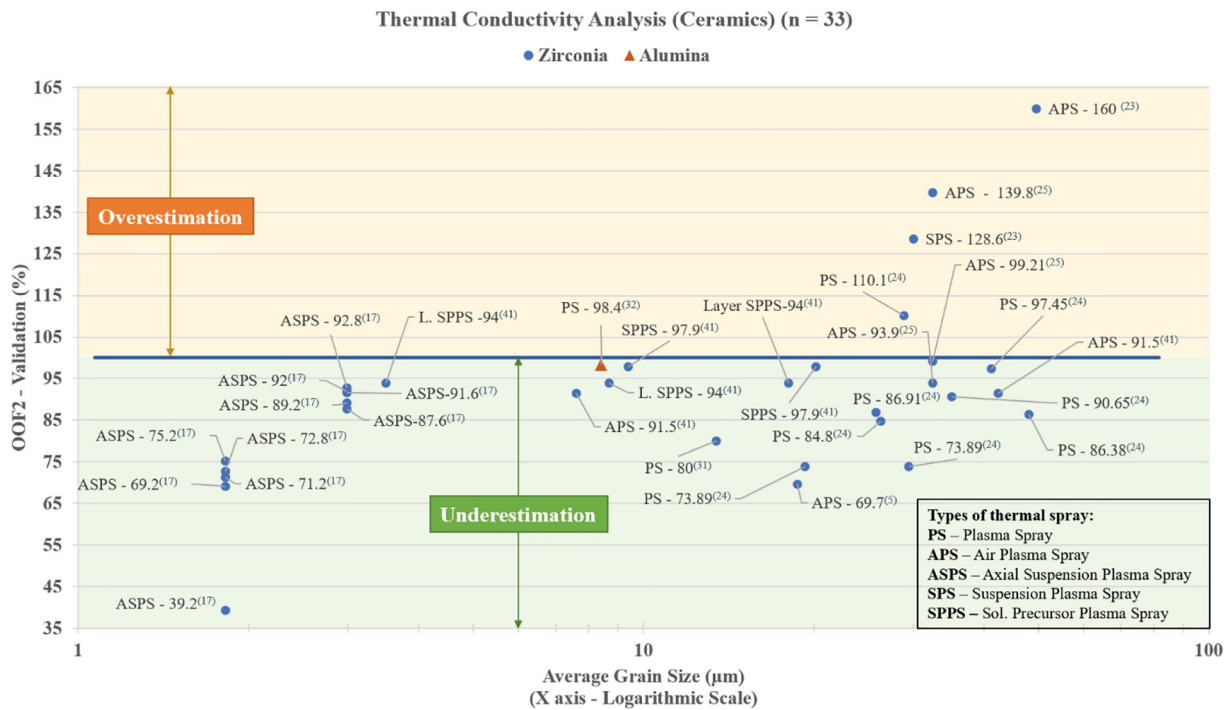


Fig. 10 OOF2 validation efficiency of thermal conductivity plotted against grain size of ceramic coatings deposited by various thermal spray techniques with the reference source of data presented in parentheses. The large range of grain sizes is presented in a

logarithmic scale in the abscissa. The predictions are more accurate for microstructures with larger grain sizes than those with smaller ones

like microstructure. In contrast, suspension and solution precursor plasma (SPS and SPPS) lead to a much finer, segmented, and denser microstructure due to the vaporization and deposition of liquid precursor passing through the plume.

OOF2 prediction of thermal conductivity of ceramics showed significant dependency on the porosity content. To explore this relationship, the OOF2 predictions of thermal conductivity are plotted against the porosity content of the ceramic coatings in Fig. 11(a). The results of solution

precursor plasma coatings (SPPS) were separated from conventional plasma-sprayed coatings, as shown in Fig. 11(b), due to the nature of the process. Conventional plasma spray utilizes solid powder particle feedstock, resulting in coatings with non-uniform porosity (Ref 5, 6). On the other hand, solution-based feedstock in SPPS yields a unique nanometer-sized microstructure with uniform porosity and cracks without injection feed problems, as the liquid medium helps reduce friction and avoid clogging issues.

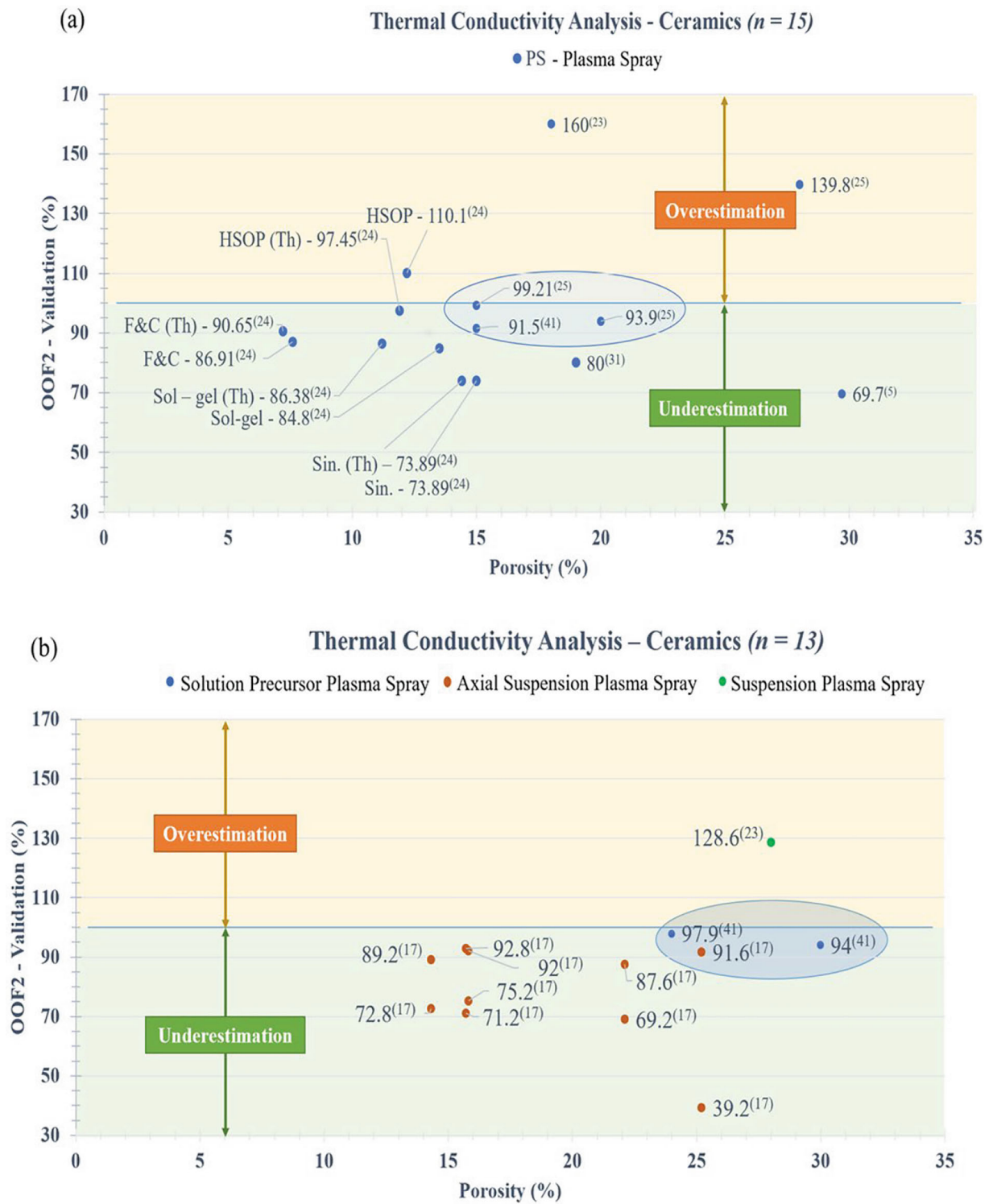


Fig. 11 Experimental data of OOF2 validation efficiency of thermal analysis plotted against the porosity percentage of ceramic coatings deposited by different thermal spray techniques with the reference source of data presented in parentheses. It is observed that OOF2 predictions are more accurate for less porous microstructures in both conventional plasma spray and solution-based plasma spray.

(a) presents all the data points obtained from the conventional plasma spraying process. It is observed that coatings with larger grain sizes and connected and free cracks result in higher efficiency despite higher porosity content. Similarly, (b) presents the data points from all the solution-based plasma spraying processes. These coatings yielded higher efficiency of OOF2 predictions

As shown in Fig. 11(a), for lower porosity percentages (5–16%), OOF2 predictions span from 70 to 110% of efficiency, whereas for large porosity percentages (18–30%), OOF2 predictions for thermal properties show a wide range underestimation and overestimation of efficiency from 70 to 160%. OOF2 validations are more accurate for less porous microstructures. Pores have a complex three-dimensional shape that cannot always be captured from a two-dimensional micrograph. As a result, the two-dimensional numerical analysis by OOF2 assumes that the pores morphology does not change in the third dimension. Thus, porosity leads to overestimation or underestimation in predicting the property value. The porosity content in the thermal sprayed coating increases the coating's interfacial and air gap resistances, affecting the thermal conductivity output solved by OOF2 analysis.

Interestingly, an outlier was observed in plasma-sprayed coatings, as highlighted in Fig. 11(a), with a blue bubble enclosing the plotted data from 15 to 20% porosity. These coatings with a higher porosity content show 92–99% efficiency in OOF2 predictions. Despite higher porosity, higher efficiency is observed because these microstructures have a larger grain size of 40–50 microns and unique connected crack and free crack microstructural features (Ref 25). 'Free cracks' are cracks that do not have connected branched crack features in the main stem of the crack. The presence of these connected and free cracks aids OOF2 in improving the identification of these heterogeneous features in the microstructural image of the coating. Fine cracks are often not identified by OOF2, resulting in lower prediction efficiency. However, it is difficult to conclude this trend since these data points come from the same article (Ref 25). The comparison needs more experimental data from OOF2 thermal analysis conducted on ceramic coatings with similar porosity deposited by other thermal spray processes.

The various kinds of powder feedstock that can be injected into the plasma plume influence the coating microstructure and OOF efficiency, as shown in Fig. 11(a). Powder feedstock can be classified into fused and crushed (F&C), hollow spherical particle (HOSP), sintered (Sin.) and solution–gel (sol–gel) based feedstock. In F&C feedstock, the material is formed with a fused solid mass, which is then mechanically crushed to obtain the smaller feedstock particle of appropriate size for deposition. The F&C feedstock is pointed and irregular-shaped sharp particles. The HOSP feedstock, although spherical in morphology, produces porous microstructure due to less dense and absence of material in the core of the particle. Sintered feedstock has high-density individual particles. The sintering process helps reduce the feedstock's porosity to obtain dense deposited coating through plasma spraying. Sol–gel feedstock consists of feedstock suspended in a

liquid medium, which aids in reduced friction during particle deposition on a substrate. Sol–gel feedstock can be adjusted to obtain a variety of microstructures, from highly porous to less porous, based on the application and requirement of the coating. OOF2 predictions have 90–97% efficiency for fused and crushed (F&C) and HOSP feedstock, sol–gel, whereas sintered feedstock shows less than 90% prediction efficiency. The higher efficiency can be linked to F&C feedstock having uniform-size powder particles (10–60 μm), which aids in the uniform melting of the feedstock through the plasma plume to produce high-density coatings. Additionally, sintered feedstock produces a coating with higher porosity in the study, which results in low efficiency in OOF2 predictions. However, the sol–gel feedstock results in interlamellar pores and intra-splat cracks in the coatings, which are not resolved at captured magnification. The presence of such cracks and pores within the bulk, when not represented in the 2D microstructure, results in less accurate OOF2 predictions (Ref 24).

While comparing the solution-based plasma spraying processes in Fig. 11(b), it is noticed that for lower porosity percentages (14–16%), OOF2 predictions span from 70 to 90% of validation, showing a significant underestimation, whereas for large porosity percentages (23–30%), OOF2 predictions for thermal properties show a wide range of validation from 40 to 130%. However, an outlier trend has also been noticed, highlighted by a blue bubble in Fig. 11(b) that encloses the experimental data of 25 to 30% porosity in the coatings. Here, the solution precursor plasma-sprayed (SPPS) coatings show exceptionally accurate OOF2 predictions of over 90 percent (Ref 39) despite higher porosity percentage. Solution-based feedstock produces a large variation in hierarchical and multiscale microstructure depending on the solution characteristics, plume injection, and subsequent interaction. Thus, solution-based coatings require multiscale imaging and OOF analysis for a more consistent and accurate prediction.

OOF Prediction of Thermal Properties in Metallic Coatings

The experimental data for the thermal properties of thermal sprayed metallic coatings, which include metals and their composites, are plotted in Fig. 12. The data consist primarily of aluminum and tungsten-based materials. A mere 5 data points were available for the thermal analysis of metallic coatings (Ref 21, 27). Vacuum plasma-sprayed tungsten shows the most accurate OOF2 predictions. The porosity percentage recorded for the tungsten coating is 7%. This higher efficiency in OOF2 predictions is because vacuum plasma spray produces the densest coating.

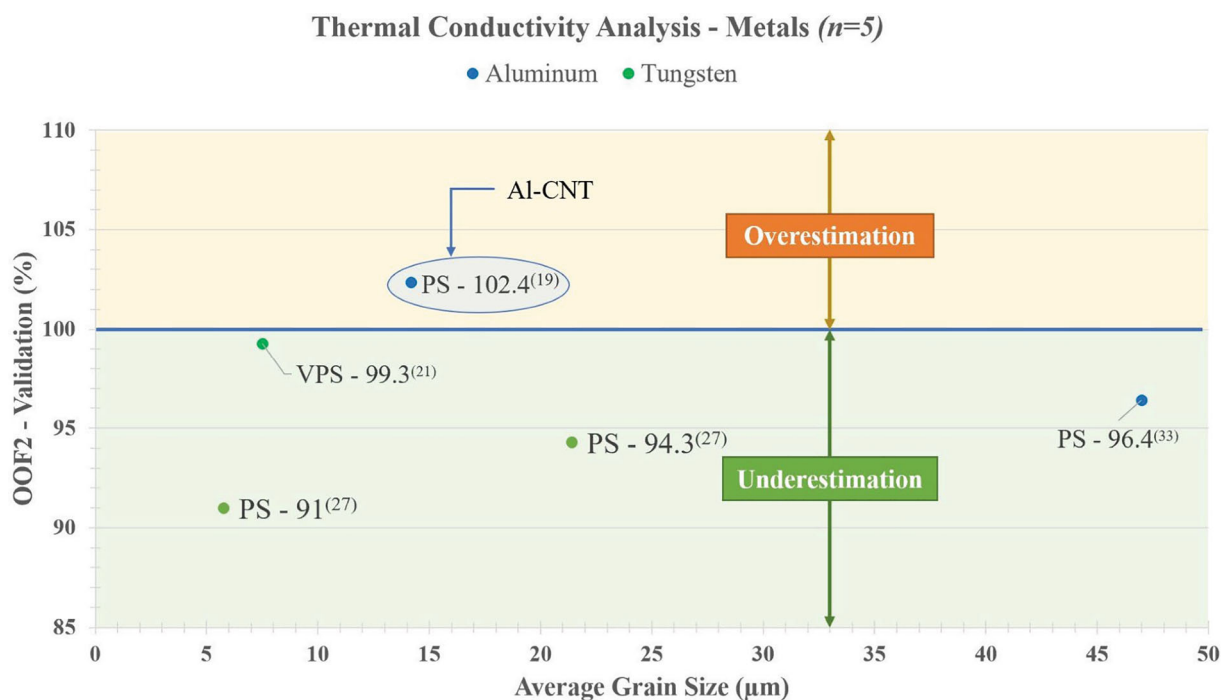


Fig. 12 Experimental data of OOF2 validation efficiency of thermal conductivity analysis of metallic thermal sprayed coatings plotted against average grain size of the microstructure with the reference source of data presented in parentheses. The metallic coatings in this plot are sprayed by plasma spray and vacuum plasma spray process.

Furthermore, as highlighted in Fig. 12, a blue bubble at 14 μm grain size showed plasma-sprayed aluminum with 10% dispersed carbon nanotubes (CNTs) in the microstructure. Despite having a smaller average grain size, the OOF2 predictions are accurate to the experimental estimations in the presence of CNTs. CNT reinforcements in the microstructure become more distinct and easier for heterogeneous phase identification in the matrix. CNTs are externally traced on the experimentally obtained microstructure to improve the detection of distinct heterogeneous phases (Ref 19). The simplified image with traced CNTs is used for the OOF analyses in the original microstructure obtained experimentally. The increased image resolution is the cause for better and more accurate predictions by OOF2 despite the smaller grain size of the microstructure. This also shows that OOF2 is a robust tool for thermal analysis on metal matrix composite coatings manufactured by thermal spray.

OOF Prediction of Mechanical Properties of Ceramic Coatings

Mechanical analysis of thermal sprayed coatings includes predicting effective elastic modulus and stress distribution in the microstructure. In OOF, the mechanical properties of the microstructure are obtained by applying tensile or

The OOF2 predictions yield more accurate results with an increase in the grain size of the microstructure. It is noted that introducing reinforcements like carbon nanotubes (CNTs) in the metal matrix increases OOF2 predictions

compressive strain, lower than the material's yield point, to the microstructure's top boundary. The bottom boundary of the microstructure is fixed in the horizontal and vertical directions. The stress contour plot of the microstructure provides stress accumulation around heterogeneous elements such as porosity, material jetting, and grain boundary. Additionally, it highlights the regions of localized higher strength in the microstructure. Figure 13 shows the percentage of validation of OOF2 predictions of the overall mechanical property of elastic modulus of thermal sprayed ceramic coatings against the average grain size of the microstructure. To present a large range of grain sizes, they are plotted on a logarithmic scale in the abscissa. Like the trend observed in the section on thermal analysis of ceramics, OOF2 predictions have improved efficiency with an increase in the average grain of the microstructure. For smaller grain sizes (10–45 μm), OOF2 predictions span from 95 to 300%, showing a large overestimation bracket, whereas, for large grain sizes (50–500 μm), OOF2 predictions for mechanical properties show increased efficiency from 95 to 110%. The resolution of the grain boundary and mesh is higher at a larger grain size, which increases the efficiency of the OOF2 predictions.

Thermal-sprayed coatings are anisotropic. Figure 13 also shows that the elastic modulus predictions are more accurate in the transverse to spray direction (denoted by 'T'

Mechanical Property Analysis – Ceramics ($n = 27$)

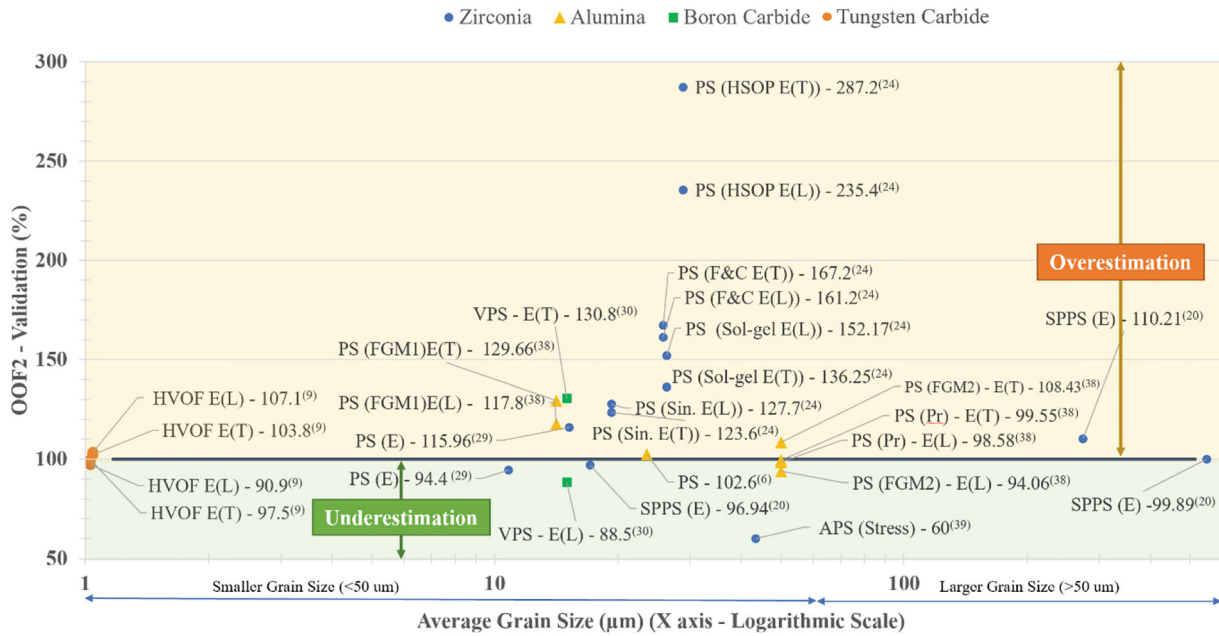


Fig. 13 Experimental data of OOF2 validation efficiency of mechanical analysis of ceramic plasma-sprayed coatings with the reference source of data presented in parentheses

beside nomenclature) than those in a longitudinal to spray direction (denoted by ‘L’ beside nomenclature). In thermal sprayed coatings, the impacting splats have different resistance to deformation in the transverse and spray direction of the coating. A high deformation load is required to deform the coating in the transverse direction as it has the adhesion strength of several layers of thermal spray deposition, and a larger number of splats are being deformed. However, a lower deformation load is required to deform or delaminate a coating along the spray direction because it contains the adhesion strength of only a single layer in the given direction. A larger number of adhered or bonded splats thus require a relatively larger amount of stress to bring about the same elastic strain as compared to the smaller number of splats. Thus, OOF2 can account for anisotropy of the microstructure by solving for stresses and strains in two different directions. These directions are then identified as longitudinal (xx) and transverse (yy) directions for the user-defined boundary conditions. To conclude, the trend of higher efficiency of OOF2 predictions in the transverse direction than in longitudinal directions needs additional experimental analysis of coating samples with a similar composition of materials subjected to the same boundary and loading conditions.

Figure 13 shows that the efficiency of OOF2 predictions for SPPS (solution-precursor plasma spray) is unaffected by the grain size of the microstructure. Even at smaller grain sizes, the prediction efficiency of modulus by OOF2 is above 97%. Such a trend is attributed to aqueous

precursor feedstock, which yields unique features in microstructure such as uniform porosity and through-thickness vertical cracks (Ref 41). The uniformity in the coating promotes higher efficiency due to the more precise identification of the different phases in the microstructure. However, more data points are required from the literature to study this trend more precisely (Ref 20).

Figure 13 also shows that these ceramic coatings have been obtained using different powder feedstock such as sol-gel-based, sintered (Sin.), fused and crushed (F&C), and hollow sphere-based (HOSP) particles. Wang et al. predicted the elastic modulus of plasma-sprayed coatings using four zirconia types: fused & crushed, sol-gel, HOSP (hollow sphere), and sintered. OOF2 predictions were most accurate for sintered zirconia feedstock and least accurate, with a high overestimation of 200-300% for HOSP feedstock (Ref 24). This divergence is because HOSP feedstock contains hollow spherical particles, which results in the unusually large porosity of splat boundaries upon thermal spraying, which was not included in the modeling. In contrast, sintered feedstock shows higher efficiency in OOF2 predictions because the porosity in the feedstock is reduced, resulting in a dense microstructure. Interestingly, the relative effect of porosity on thermal conductivity and elastic modulus of the bulk is not equivalent. Thermal conductivity is more sensitive to porosity percentage owing to the Kapitza effect. Thus, a bulk deposit with identical porosity will have a higher OOF2 prediction efficiency for mechanical properties than thermal.

OOF Prediction of Mechanical Properties of Metallic Coatings

OOF predictions of the mechanical properties of thermal sprayed metallic coatings were plotted against the average grain size of the microstructure in Fig. 14. OOF2 predictions were more accurate for larger grain sizes ($>20\ \mu\text{m}$) compared to the smaller grain size ($< 20\ \mu\text{m}$) due to improved image resolution, a trend like thermal properties validation.

As observed in Fig. 14, the wire arc-sprayed Inconel coatings with larger grain size show an overestimation with 125-135% validation with the reported porosity of 6%. Furthermore, OOF2 predictions for these Inconel coatings have 5% higher efficiency in the transverse direction than in the longitudinal direction. These observations are in good agreement with the trend discussed for thermal property analysis. The larger grain size and low porosity yield higher efficiency in the OOF2 predictions. The better prediction in the transverse direction results from higher adhesion of coatings in the transverse direction than in the longitudinal direction (Ref 12). Additionally, it is observed that OOF2 predictions for the Wire arc-sprayed Zn-Al metallic coatings with smaller grain size show an underestimation in efficiency with 65-75% validation with the reported porosity of $7.35 \pm 0.93\%$ (Ref 11). This could be due to poor resolution and sharpness of microstructure, which prevents accurate detection of features like grain

boundaries, cracks, and porosity in the Zn-Al coating for OOF2 analysis. However, an outlier is detected from the trend where the Zn-Al coating shows a 10% lower prediction efficiency in the transverse direction than in the longitudinal direction. Upon examining the microstructure, it was observed that the porosities and wide grain boundaries were concentrated in a vertical plane in the transverse direction in Zn-Al coatings. These porosities and boundaries are more evenly distributed when observed longitudinally. Thus, an accumulation of porosity in the transverse direction could reasonably impair the OOF2 predictions compared to that in the longitudinal direction (Ref 9-11).

Following that, the HVOF and plasma spray processes show the most accurate OOF2 predictions. Plasma-sprayed Inconel and tungsten carbide-cobalt alloys (WC-Co), as shown in Fig. 14, have a large grain size greater than $20\ \mu\text{m}$ (Ref 35), resulting in higher efficiency of OOF2 predictions. However, it is noticed that HVOF-sprayed WC-Co alloy, despite a smaller grain size of $1\ \mu\text{m}$, shows the highest prediction efficiency. This can be linked to very low porosity in bulk, i.e., 2.86%, accounting for a highly dense microstructure. Lower porosity yields higher efficiency of OOF2 predictions (Ref 8).

It is striking to note that the cold-sprayed tungsten deposits with 10% and 17% reinforced cobalt yield the least accurate results, with an overestimated 200-400% (Ref 15). Such large divergence from experimental validation could be due to the poor microstructure image

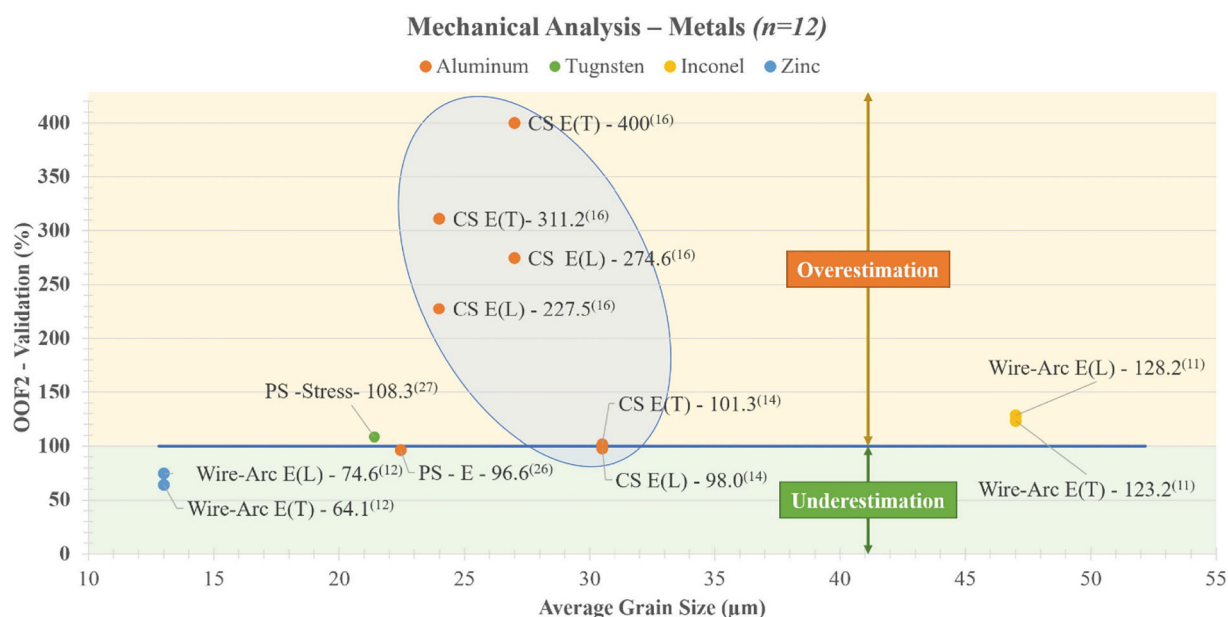


Fig. 14 Experimental data of OOF2 validation efficiency of mechanical analysis of metallic thermal sprayed coatings plotted against average grain size of the microstructure with the reference source of data presented in parentheses. The overall effective modulus of the coatings is numerically analyzed using OOF2. These coatings are obtained through Plasma spray, HVOF, wire_arc, and cold spray

processes. The OOF2 predictions yield more accurate results with an increase in the grain size of the microstructure. It is observed that the deposition of cold-sprayed coatings with a higher weight percent of metal matrix composite and HVOF-sprayed coatings results in the most accurate OOF2 predictions

selection and the higher porosity content. The data on microstructural features, such as the porosity content of the coatings, are not reported consistently in the literature. There should be more comparable data to make notable predictions of the trends observed in cold-sprayed deposits to derive more significant conclusions (Ref 15).

However, for the aluminum cold-sprayed deposits, the OOF2 prediction is significantly improved to a higher validation efficiency of 98–101%. This boost in efficiency results from an increase in zinc content in the aluminum matrix. Notably, the volume percentage of zinc in aluminum coatings is 8–15% more than cobalt in tungsten coatings (Ref 15). The addition of zinc increases the heterogeneity of the Al-Zn coating, which improves the resolution of the microstructure. Additionally, the reported porosity for the Al-Zn matrix is $1.26 \pm 0.18\%$, producing a very dense microstructure for OOF2 analysis. Thus, the increased heterogeneity and low porosity yield higher efficiency in OOF2 predictions of Al-Zn coatings (Ref 14).

Guidebook on OOF2 Prediction of Properties in Thermal Sprayed Coatings

It can be understood from the results and discussions that the agreement (or absence thereof) of OOF2 calculations of properties of thermal sprayed coatings with those obtained from experimental measurements is a *complex interplay* between structure, processing, and properties of the coatings. In order to simplify this landscape, this section creates a “guidebook” for new users to employ OOF2 by understanding the relative importance of key input features and the extent to which they play a role in the accuracy of calculated outputs.

The magnification at which the microstructure is captured plays a crucial role in OOF2 analysis. The OOF2 software can accommodate input data as experimental acquired or computationally generated artificial microstructures. Experimental microstructure images of thermal spray process deposition techniques are commonly obtained using optical or electron microscopy. Typically, as presented in Fig. 15, magnifications range from $100\times$ to $1000\times$ for optical microscopy (OM), $1000\times$ to $20,000\times$ for scanning electron microscopy (SEM), and beyond $20,000\times$ for transmission electron microscopy (TEM) (Ref 1). For thermal spray applications, OOF2 predictions are most accurate within the range of $1000\times$ to $20,000\times$. The significant coating features may be under-resolved at lower magnifications, leading to inaccurate property predictions. Conversely, OOF2 may over-resolve the microstructure at higher magnifications, detecting artificial features due to pixelation and missing other hierarchical features.

In multiscale analysis, the representative volume element (RVE) represents a portion of the material system that

accurately reflects its overall behavior. It is a valuable tool for understanding complex materials systems (Ref 43). The global RVE model focuses on larger areas of the coating, evaluating inter-splat interactions, while the local RVE model examines specific features like individual splats and large porosities to assess their influence on the coating. The optimal magnification for resolving the microstructure depends on the process and is determined through RVE analysis. For example, HVOF and wire arc-sprayed coatings resolve at magnifications as low as $300\times$ – $500\times$. Plasma-sprayed and cold-sprayed coatings exhibit precise representations at 1000 – $15,000\times$ magnifications. It is crucial to select the appropriate magnification range for accurate analysis, as lower magnifications may lead to under-resolved features, while higher magnifications can introduce artifacts. The multiscale approach using representative volume elements (RVEs) allows for the evaluation of inter-splat interactions and the influence of individual features on the overall coating properties. OOF2 increases prediction accuracy with higher magnifications, facilitating comprehensive assessments of heterogeneous coatings.

Moving on from magnification to structural variables, the most important ones include grain size and porosity, spraying process and feedstock density, and properties related to splat anisotropy. The deviation of OOF2 calculations from experimental measurements is divided into agreement, underestimation, and overestimation, with a summarized schematic presented in Fig. 16(a). Since OOF2 is a microstructure-based modeling tool, corresponding features, such as grain size and porosity, have a relatively larger effect on its prediction efficiency. The spread of deviation is also the largest. In comparison, feedstock density and processing have a lower impact on prediction efficiency. However, higher-density feedstock particles and higher-velocity spraying processes fare better. It thus suffices to deduce that for all spraying techniques, OOF2 accomplishes a reasonably agreeable prediction limited only by the quality of microscopic characterization. Finally, calculations along the transverse directions are more agreeable than those in the longitudinal one for reasons explained earlier.

Based on this summary, an index of parameters acquired as input by the researcher for OOF2 simulation can be itemized. These are ranked, from high to low, according to their relative importance for obtaining an accurate validation efficiency against experimental measurements, as shown in Fig. 16(b). Grain size captures the top spot, followed closely by porosity and second phase content such as precipitates and reinforcements at 2nd and 3rd, respectively. Of course, related features such as cracks also play an important role. It is thus recommended to acquire microstructural images at multiple scales, with larger scales capturing grains and small ones capturing intra-granular characteristics. Feedstock density comes 4th in importance, with the spraying process at

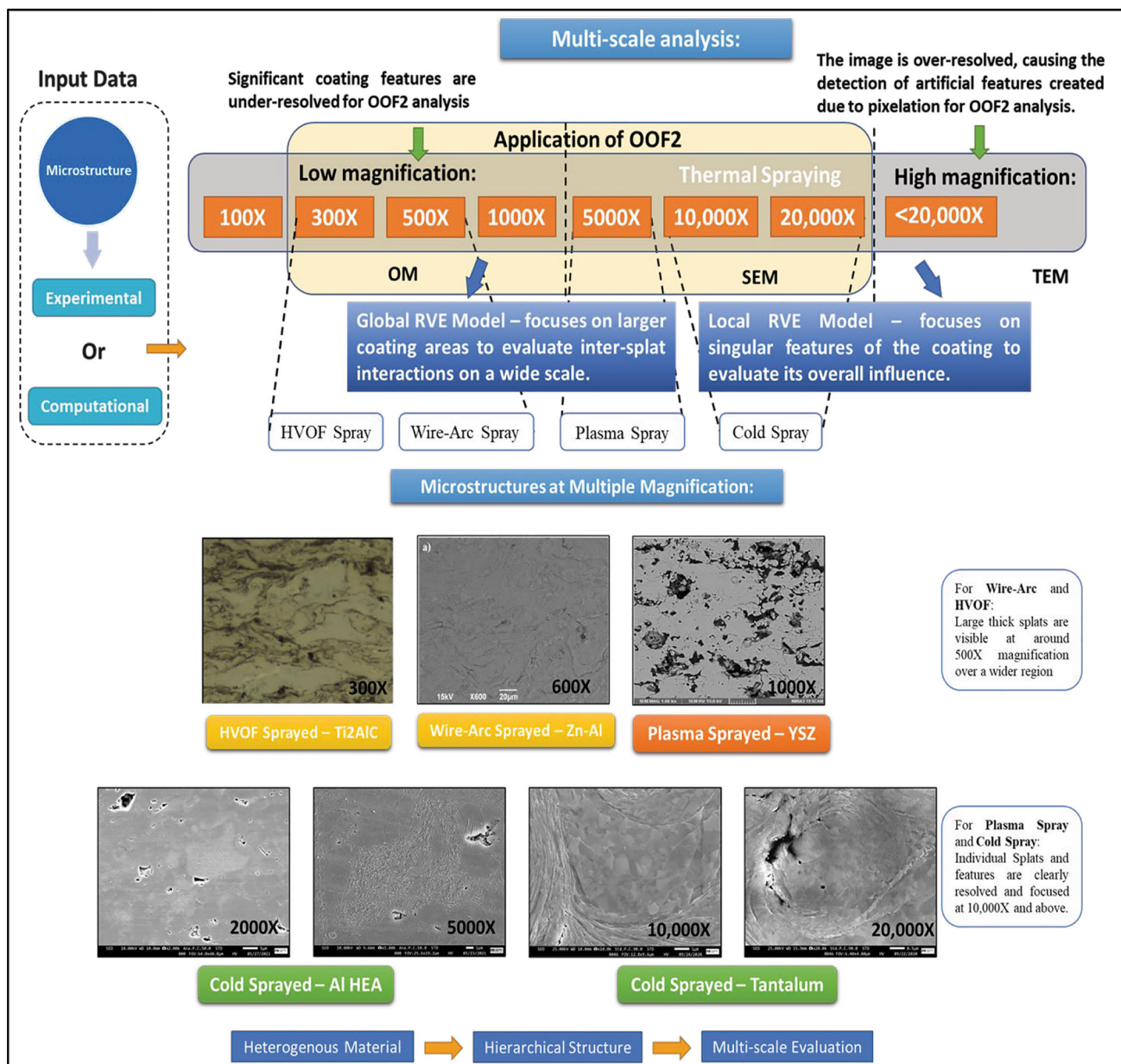


Fig. 15 Schematic explanation for microstructure-based analysis using OOF2 software enables comprehensive evaluation of thermal sprayed coatings at different length scales, incorporating features captured from microscopy techniques or computationally generated structures

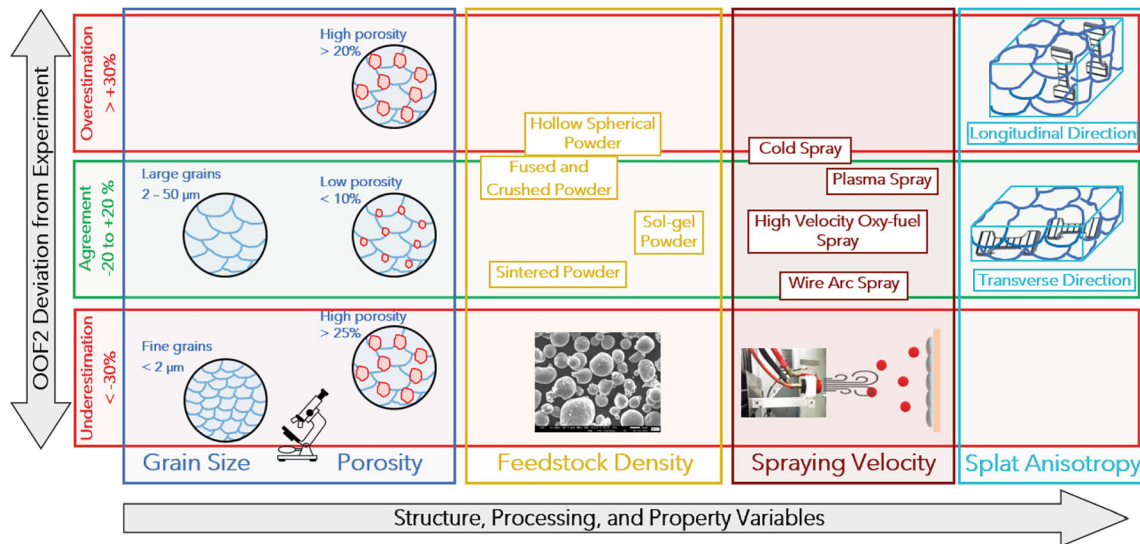
5th. It is noted that they cannot be isolated as spraying velocity and feedstock density determine the grain size and porosity. Finally, in 6th place is the direction of testing anisotropy in transverse or longitudinal. Thus, despite a limited 37 articles in the literature, this summary schematic and ranking serve as a guideline to researchers for understanding the relative roles of various parameters in OOF2 calculations of thermal and mechanical properties on thermal sprayed coatings. Acquiring the inputs in this order of importance, integrated with the overall characterization, is expected to improve the efficiency of OOF2 validation. This schematic serves as a guideline to researchers for understanding the

relative roles of various parameters in OOF2 calculations of thermal and mechanical properties on thermal sprayed coatings.

Conclusion

The analytical critique establishes a landscape of predicting thermal and mechanical properties of thermally sprayed coatings by object-oriented finite element modeling using OOF2. Inferences are drawn from a review and data mining of 37 research articles published on microstructure-based

(a) Landscape of OOF2 Validation on Thermal Sprayed Coatings



(b) Ranked Importance of Input Acquisition Parameters

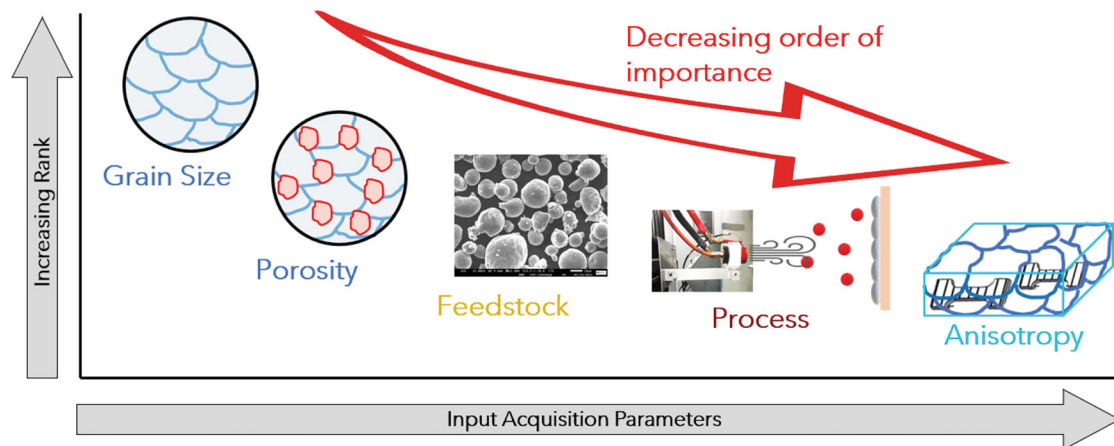


Fig. 16 (a) Landscape of OOF2 validations on thermal and mechanical properties of thermal sprayed coatings compared to their experimental measurements. (b) Significance and impact of input acquisition parameters on OOF2 validation ranked in decreasing order of importance

finite element modeling of these coatings. The thermal and mechanical properties calculated by OOF2 are compared with experimentally acquired results. The efficiency of OOF2 in predicting these properties and its dependence on microstructural features, such as length scale or magnification, grain size, porosity, and composition, are presented. Overall, all observations reinforce that the quality of microstructural images acquired and the ability to distinguish heterogeneities in those images determine the validation efficiency of OOF2 predictions. Large grain sizes yield higher efficiency of OOF2 predictions as they exhibit higher resolution at the same length scale than smaller grains. The higher resolution results in better local microstructural features such as grain boundaries, reinforcements, cracks, and porosities. The ease of defining mesh boundaries and assignment of local properties, in

turn, boosts the efficiency of OOF2 predictions. Specifically, higher porosity leads to lower prediction efficiencies in the thermal analysis of thermally sprayed coatings. While porosity is a non-uniform 3D microstructural feature, OOF2 computes a 2D image. The assumption of the continuity of this 2D image in the third dimension deviates from the calculated values from the experimentally acquired results. It is recommended to report porosity as key data of the microstructures in all the articles to develop a comprehensive knowledge of the predictions by OOF2. Furthermore, it was noted that performing analysis at multiple length scales instead of a single scale provides the coating quality information on local and bulk levels throughout the microstructure.

There are a few exceptions where microstructure obtained from SPPS sprayed coating has shown more

accurate OOF2 predictions even at smaller grain sizes and higher porosity content in the microstructure. OOF2 predictions for mechanical analysis of thermal sprayed coatings show higher efficiency in the transverse direction than in the spray direction due to the higher coating resistance against deformation. The data from these articles indicate that OOF2 predictions were most accurate for plasma-sprayed coatings. However, it is not trivial to rank the thermal processes since only three studies focus on wire-arc-sprayed, HVOF, and cold-sprayed coatings, respectively, and 28 articles were published on plasma-sprayed deposits. Thus, it is expected that with the growing application of the OOF2 technique and thermal spray-based additive manufacturing approaches, there will be a continued increase in OOF-based reports. This study demonstrates the potential of image-based finite element analysis performed by OOF2 to obtain a high-quality thermal sprayed coating with optimized parameters, benefiting the thermal spray community.

Supplementary Information The online version contains supplementary material available at <https://doi.org/10.1007/s11666-024-01797-1>.

Acknowledgments The authors gratefully acknowledge support from the DEVCOM_Army Research Laboratory—through the W911NF2020256 grant.

Data Availability The data files for microstructure images mentioned in the ‘Grain Size Measurement’ section are available on GitHub at https://github.com/rjoshio20/OOF2-Microstructures-Images_

References

1. P. Vuoristo, *Thermal spray coating processes, comprehensive materials processing*, Vol 4 Elsevier, Amsterdam, 2014.
2. S. Seal, S.C. Kuiry, P. Georgieva, and A. Agarwal, Manufacturing Nanocomposite Parts: Present Status and Future Challenges, *MRS Bull.*, 2004, **29**(1), p 16-21.
3. R. Patel, A. Keshri, G. Dulikravich, and A. Agarwal, An experimental and computational methodology for near net shape fabrication of thin-walled ceramic structures by plasma spray forming, *J. Mater. Process. Technol.*, 2010, **210**(10), p 1260-1269.
4. OOF: Finite Element Analysis of Microstructures, NIST. Accessed Aug 2021
5. K. Torkashvand, E. Poursaeidi, and J. Ghazanfarian, Experimental and Numerical Study of Thermal Conductivity of Plasma-Sprayed Thermal Barrier Coatings with Random Distributions of Pores, *Appl. Therm. Eng.*, 2018, **137**, p 494-503.
6. S. Bhusal, C. Zhang, J. Bustillos, P. Nautiyal, B. Boesl, and A. Agarwal, A Computational Approach for Predicting Microstructure and Mechanical Properties of Plasma-Sprayed Ceramic Coatings from Powder to Bulk, *Surf. Coat. Technol.*, 2019, **374**, p 1-11.
7. K. Balani and A. Agarwal, Process map for plasma sprayed aluminum oxide-carbon nanotube nanocomposite coatings, *Surf. Coat. Technol.*, 2008, **202**(17), p 4270-4277.
8. R. Ghafouri-Azar, J. Mostaghimi, and S. Chandra, Modeling Development of Residual Stresses in Thermal Spray Coatings, *Comput. Mater. Sci.*, 2006, **35**(1), p 13-26.
9. G. Bolelli, A. Candeli, H. Koivuluoto, L. Lusvarghi, T. Manfredini, and P. Vuoristo, Microstructure-Based Thermo-Mechanical Modelling of Thermal Spray Coatings, *Mater. Des.*, 2015, **73**, p 20-34.
10. J. Jiang and P. Nyllén, Object-Oriented Finite Element Analysis to Simulate Microindentation of Thermal Sprayed MAX-Phase Coatings. In: Proceedings - 2009 International Conference on Computer Modeling and Simulation, ICCMS 2009, 2009, 337-341.
11. C. Leither, J. Risan, M. Bashirzadeh, and F. Azarmi, Determination of the Elastic Modulus of Wire Arc Sprayed Alloy 625 Using Experimental Analytical, and Numerical Simulations, *Surf. Coat. Technol.*, 2013, **235**, p 611-619.
12. A. Darabi and F. Azarmi, Investigation on Relationship Between Microstructural Characteristics and Mechanical Properties of Wire-Arc-Sprayed Zn-Al Coating, *J. Therm. Spray Technol.*, 2020, **29**(1-2), p 297-307.
13. T. Paul, R. Joshi, C. Walde, C. Zhang, A. Birt, M. Pepi, and A. Agarwal, Multiscale Elastic Behavior of Cold Sprayed Refractory Metal from Splat to Bulk Deposit by Integrated Experimental and Modeling Approach, *Mater. Sci. Eng. A*, 2022, **853**, p 143751.
14. A. Darabi and F. Azarmi, Validation of Methods to Measure the Hardness and Elastic Modulus of Cold-Sprayed Al-ZN Composite Coatings, *J. Mater. Eng. Perform.*, 2020, **29**(4), p 2144-2152.
15. G. Bolelli, S. Dosta, L. Lusvarghi, T. Manfredini, J.M. Guilemany, and I.G. Cano, Building up WC-Co Coatings by Cold Spray: A Finite Element Simulation, *Surf. Coat. Technol.*, 2019, **374**, p 674-689.
16. M. Bashirzadeh, F. Azarmi, C.P. Leither, and G. Karami, Investigation on Relationship between Mechanical Properties and Microstructural Characteristics of Metal Matrix Composites Fabricated by Cold Spraying Technique, *Appl. Surf. Sci.*, 2013, **275**, p 208-216.
17. A. Ganvir, C. Kumara, M. Gupta, and P. Nylen, Thermal Conductivity in Suspension Sprayed Thermal Barrier Coatings: Modeling and Experiments, *J. Therm. Spray Technol.*, 2017, **26**(1-2), p 71-82.
18. S. Kuroda, J. Kawakita, M. Watanabe, and H. Katanoda, Warm Spraying - A Novel Coating Process Based on High-Velocity Impact of Solid Particles, *Sci. Technol. Adv. Mater.*, 2008, **9**(3), p 033002.
19. S.R. Bakshi, R.R. Patel, and A. Agarwal, Thermal Conductivity of Carbon Nanotube Reinforced Aluminum Composites: A Multiscale Study Using Object-Oriented Finite Element Method, *Comput. Mater. Sci.*, 2010, **50**(2), p 419-428.
20. K. Balani, R.R. Patel, A.K. Keshri, D. Lahiri, and A. Agarwal, Multiscale Hierarchy of Chelydra Serpentina: Microstructure and Mechanical Properties of Turtle Shell, *J. Mech. Behav. Biomed. Mater.*, 2011, **4**(7), p 1440-1451.
21. A. Zivelonghi, F. Cernuschi, C. Peyrega, D. Jeulin, S. Lindig, and J.H. You, Influence of the Dual-Scale Random Morphology on the Heat Conduction of Plasma-Sprayed Tungsten via Image-Based F.E.M., *Comput. Mater. Sci.*, 2013, **68**, p 5-17.
22. G. Bolelli, V. Cannillo, L. Lusvarghi, T. Manfredini, and M. Montorsi, Glass-Alumina Composite Coatings by Plasma Spraying Part II: Microstructure-Based Modeling of Mechanical Properties, *Surf. Coat. Technol.*, 2006, **201**(1-2), p 474-486.
23. W.U. de Goes, N. Markocsan, and M. Gupta, Microstructural Changes in Suspension Plasma-Sprayed TBCs Deposited on Complex Geometry Substrates, *Coat. MDPI AG*, 2020, **10**(7), p 699.
24. Z. Wang, A. Kulkarni, S. Deshpande, T. Nakamura, and H. Herman, Effects of Pores and Interfaces on Effective Properties of Plasma-Sprayed Zirconia Coatings, *Acta Mater.*, 2003, **51**(18), p 5319-5334.

25. M. Gupta, N. Curry, P. Nylén, N. Markocsan, and R. Vaßen, Design of Next Generation Thermal Barrier Coatings—Experiments and Modelling, *Surf. Coat. Technol.*, 2013, **220**, p 20-26.
26. N. Raghukiran, A.K. Mohamed, and R. Kumar, Study of the Influence of Silicon Phase Morphology on the Microstructural Stress Distribution in Al-Si Alloys Using Object-Oriented Finite Element Modeling, *Adv. Eng. Mater.*, 2014, **16**(1), p 112-121.
27. A. Zivelonghi, A. Brendel, S. Lindig, S. Nawka, B. Kieback, and J.H. You, Microstructure-Based Analysis of Thermal- and Mechanical Behaviors of W/CuCrZr Composites and Porous W Coating, *J. Nucl. Mater.*, 2011, **417**, p 536-539.
28. G. Li, C. Wang, H. Zhang, M. Zhuang, Z. Hu, Y. Liu, and L. Wang, Preliminary Design of a Novel AlN-Al Composite Coating used for Micro-Electronic Packaging Via Finite Element Modeling, *Mater. Lett.*, 2020, **280**, p 128598.
29. P. Michlik and C. Berndt, Image-Based Extended Finite Element Modeling of Thermal Barrier Coatings, *Surf. Coat. Technol.*, 2006, **201**(6), p 2369-2380.
30. H.R.S. Jazi, F. Azarmi, T.W. Coyle, and J. Mostaghimi, Study of the Relationship Between the Young's Modulus and Microstructure of Vacuum Plasma Sprayed Boron Carbide, *Mech. Prop. Perform. Eng. Ceram. Compos. Ceram. Eng. Sci. Proc.*, 2008, **26**(2), p 235-244.
31. J.H. Qiao, R. Bolot, H. Liao, P. Bertrand, and C. Coddet, A 3D Finite-Difference Model for the Effective Thermal Conductivity of Thermal Barrier Coatings Produced by Plasma Spraying, *Int. J. Therm. Sci.*, 2013, **65**, p 120-126.
32. N. Ferguen, Y. Lahmar, Y. Fizi, R. Lakhdari, W. Leclerc, and M. Guessasma, "Surface Protection for Enhanced Performance Modeling and Prediction of the Effective Thermal Conductivity of Thermal Barrier Coatings Using FFT and FE Approaches," n.d.
33. R. Bolot, J.L. Seichepine, J.H. Qiao, and C. Coddet, Predicting the Thermal Conductivity of AlSi/Polyester Abradable Coatings: Effects of the Numerical Method, *J. Therm. Spray Technol.*, 2011, **20**, p 39-47.
34. M. Gupta, P. Nylén, and J. Wigren, A Modelling Approach to Designing Microstructures in Thermal Barrier Coatings, *J. Ceram. Sci. Technol.*, 2013, **4**(2), p 85-92.
35. F. Azarmi, T. Coyle, and J. Mostaghimi, Young's Modulus Measurement and Study of the Relationship between Mechanical Properties and Microstructure of Air Plasma Sprayed Alloy 625, *Surf. Coat. Technol.*, 2009, **203**(8), p 1045-1054.
36. A.D. Jadhav and N.P. Padture, Padture, Mechanical Properties of Solution-Precursor Plasma-Sprayed Thermal Barrier Coatings, *Surf. Coat. Technol.*, 2008, **202**(20), p 4976-4979.
37. C. Bartuli, L. Lusvarghi, T. Manfredini, and T. Valente, Thermal Spraying to Coat Traditional Ceramic Substrates: Case Studies, *J. Eur. Ceram. Soc.*, 2007, **27**(2-3), p 1615-1622.
38. V. Cannillo, L. Lusvarghi, C. Siligardi, and A. Sola, Prediction of the Elastic Properties Profile in Glass-Alumina Functionally Graded Materials, *J. Eur. Ceram. Soc.*, 2007, **27**(6), p 2393-2400.
39. C.-H. Hsueh and E.R. Fuller, Residual Stresses in Thermal Barrier Coatings: Effects of Interface Asperity Curvature/Height and Oxide Thickness, *Mater. Sci. Eng.*, 2000, **283**(1-2), p 46-55.
40. C.-H. Hsueh, J.A. Haynes, M.J. Lance, P.F. Becher, M.K. Ferber, E.R. Fuller, S.A. Langer, W.C. Carter, and W.R. Cannon, Effects of Interface Roughness on Residual Stresses in Thermal Barrier Coatings, *J. Am. Ceram. Soc.*, 1999, **82**(4), p 1073-1075.
41. A.D. Jadhav, N.P. Padture, E.H. Jordan, M. Gell, P. Miranzo, and E.R. Fuller, Low-Thermal-Conductivity Plasma-Sprayed Thermal Barrier Coatings with Engineered Microstructures, *Acta Mater.*, 2006, **54**(12), p 3343-3349.
42. H.I. Faraoun, J.L. Seichepine, C. Coddet, H. Aourag, J. Zwick, N. Hopkins, D. Sporer, and M. Hertter, Modelling Route for Abradable Coatings, *Surf. Coat. Technol.*, 2006, **200**(22-23), p 6578-6582.
43. L. Cheng and G.J. Wagner, A Representative Volume Element Network (RVE-Net) for Accelerating RVE Analysis, Microscale Material Identification, and Defect Characterization, *Comput. Methods Appl. Mech. Eng.*, 2022, **390**, p 114507.

Publisher's Note Springer Nature remains neutral with regard to jurisdictional claims in published maps and institutional affiliations.

Springer Nature or its licensor (e.g. a society or other partner) holds exclusive rights to this article under a publishing agreement with the author(s) or other rightsholder(s); author self-archiving of the accepted manuscript version of this article is solely governed by the terms of such publishing agreement and applicable law.